Paper:
Wint, N., Bennett, A., Williams, G. & McMurray, H. (2018). The Effect of Phase Continuity on the Cathodic Delamination Resistance of Polyaniline Based Coatings. *Journal of The Electrochemical Society, 165*(13), C890-C899.
http://dx.doi.org/10.1149/2.0801813jes

The Effect of Phase Continuity on the Cathodic Delamination Resistance of Polyaniline Based Coatings.

N. Wint,[z] A. Bennett, G. Williams, and H. N. McMurray[*]

Materials Research Centre, College of Engineering, Swansea University, Crymlyn Burrow, Swansea SA1 8EN, United Kingdom

*Electrochemical Society Member.

[z]E-mail: n.wint@swansea.ac.uk

Abstract: Organic coatings based on electrically conducting polyaniline emeraldine salts (ES) and electrically insulating polyvinyl butyral (PVB) are applied to an iron substrate. An investigation is made into how ES phase continuity, and in-coating charge percolation, affect the kinetics and mechanism of corrosion driven cathodic coating delamination. Bilayer coatings are prepared by solution casting continuous ES films onto the substrate, then overcoating with PVB. These are compared with composite coatings of decreased phase continuity, prepared using ES powders dispersed in PVB. Coating delamination is followed using scanning Kelvin probe potentiometry and optical spectrophotometry. At ES coating weights < 0.05 $mg.cm^{-2}$, delamination rate was inversely proportional to coating weight and slower for bilayer coatings. The same trend was found at higher coating weights for ES doped using camphorsulfonic acid. However, for ES doped with phenylphosphonic acid, bilayer coating delamination rates became independent of ES coating weight > 0.05 $mg.cm^{-2}$ and were greater than for dispersion coatings. The relationship between cathodic delamination rate and PAni ES continuity is proposed to depend strongly upon the nature

and continuity of the interphase formed between the PAni ES coating and iron, and therefore on the dopant anion identity.

This was Paper 881 presented at the Washington, DC, Meeting of the Society, October 7-12, 2007.

1. Introduction

Intrinsically conducting polymers (ICPs), [1-13] including polyaniline (PAni), have been the subject of numerous studies aimed at meeting the industry-wide need to find cost effective, stable and efficient inhibitors of corrosion-driven coating delamination.[14-17] However, much debate exists regarding the effectiveness of ICPs as alternatives to chromate based corrosion inhibitors. Coatings based on ICPs have previously been found to fail, and in some cases have caused the acceleration of corrosion. [8] The effectiveness of ICPs is generally believed to be dependent on their form, and the nature of the environment. Further understanding of the reasons behind coating failing are therefore needed to aid in the development of improved protective coatings.

PAni exists in several states, which are related by the redox and acid-base equilibria shown in Figure 1.[12] The emeraldine salt of PAni (PAni ES) is electrically conducting and is the form most commonly used in corrosion-protective applications. PAni ES is produced by protonation of the emeraldine base (PAni EB) using a Bronsted acid 'dopant' such as phosphoric, [18] oxalic, [18] phosphonic, [19-20] hydrochloric, [21-22] perchloric, [23] sulphuric [23] or sulfonic acids [18-19, 22-26] via Equation (1).

$$PAni\ EB + H\ Dopant \leftrightharpoons PAni\ Dopant \quad (1)$$

When coated onto steel (iron), the corrosion resistance offered by PAni ES has previously been attributed to substrate enoblement and formation of a passive oxide film.[1-2] Substrate

potential values within the passive regime are believed to become established through electron transfer with the ES/ leuco base (LB) redox couple [2] (shown in Figure 1) for which E^0 values of between (0.22 ± 0.08) V and (0.4 ± 0.18 V) vs. SHE have been reported. [23] Under atmospheric conditions, substrate potentials can remain ennobled over an indefinite period of time due to the cyclic re-oxidization of PAni LB by atmospheric O_2, as shown schematically in Figure 2 [12].

(Figure 1)

(Figure 2)

The rate of the cathodic oxygen reduction reaction (COR) may become suppressed at the PAni ES ennobled substrate potential, thereby reducing rates of corrosion-driven cathodic coating delamination.[12, 27] Variation in the performance of PAni ES coatings has therefore been attributed to the dependence of PAni ES redox potential on the identity of the dopant anion [12, 23] and the anion-dependence of the oxide and salt films formed at the coating-iron interface. [12] However, it has been shown elsewhere that PAni ES can act as an effective smart release coating for dopant anions with corrosion inhibitor properties such as anionic organic inhibitors of the COR. [27]

During cathodic coating delamination, ES becomes converted to emeraldine base (EB), a process which can occur via either direct chemical de-doping, via the reverse of reaction (1), or via electrochemical reduction to PAni LB, and atmospheric re-oxidation to PAni EB. [12] During the reduction of an acid doped ICP, either dopant anion ejection or electrolyte cation uptake must occur in order to allow maintenance of charge neutrality. [28] The active area of the polymer in contact with the electrolyte is therefore of importance, as is the in-coating mobility of the dopant anion. [28] Under immersion conditions, it has been found that

some ICPs are able to passivate small defects, whilst the presence of large defects has led to coating failure. [29-30] In comparison, under atmospheric conditions, the length scale over which the reduction front proceeds, for the release of the same amount of inhibitor, is over several 100 micrometers as compared to approximately one micron (film thickness). [28] The effectiveness of the coating is then dependent on both electrolyte cation, and dopant anion, mobility. During a study of cathodic coating delamination, it has previously been shown that continuous conducting coatings composed of polypyrole doped with sulfonic acid are susceptible to fast breakdown (reduction) as a result of high cation mobility in the reduced polymer. [28] The same study suggested that this type of coating breakdown would also occur in the case of conducting polymers dispersed in a non-conducting matrix under circumstances where high levels of electrical conductivity are attained due to the presence of extended percolation networks of the conducting polymer phase. [28]

The current work aims to build upon the findings obtained in the case of polypyrole, by better determining the role of PAni ES phase continuity on the rate of corrosion-driven cathodic delamination for PAni ES based coatings. In so doing, the delamination of solid homogeneous films of PAni ES of varying thickness, overcoated with an electrically non-conducting polyvinybutyral (PVB) lacquer (which from herein will be referred to as PVB/PAni ES bilayer coatings), have been investigated using a combination of the scanning Kelvin probe (SKP) potentiometry, [12] and optical spectrophotometry. The results thus obtained are compared with those obtained using coatings containing varying volume fractions of PAni ES powder dispersed in PVB [12] (which from this point forward will be referred to as PVB/PAni ES dispersion coatings). The ability to follow cathodic delamination of thin PAni films from metal substrates, by exploiting the dissimilar optical

absorbance spectra (colours) of the varying PAni redox and acid-base states, has been shown elsewhere. [31]

The identity of the dopant acid has previously been shown to influence the susceptibility of PVB/PAni ES coatings to cathodic delamination. [12] For this reason, the performance of PAni ES doped using phenylphosphonic acid (H_2PP) has been compared with that doped using camphorsulfonic acid (HCS) in both the bilayer and dispersion coatings. In so doing, our aim has been to better determine how the chemical nature and physical continuity of the interphase, [12, 32] which forms as a result of reaction between the PAni ES and the substrate metal, affect coating delamination resistance.

2. Experimental

Materials: Coupons of iron foil of 1.5 mm thickness and 99.5 % purity were obtained from Goodfellow Cambridge Ltd. Polyvinyl butyral-co-vinyl alcohol-co-vinylacetate (PVB), molecular weight 70,000 – 100,000 Da, polyaniline emeraldine base (PAni EB), molecular weight ca. 6500 Da, HCS, H_2PP and all other chemicals were obtained from Sigma Aldrich Chemical Co. at analytical grade purity.

Methods:

Samples of iron foil were ground to a European P grade P1200 grit finish using silicon carbide (SiC) abrasive paper and were cleaned and degreased using ethanol and distilled water before experimentation. Glass substrates were degreased using ethanol.

Solutions of PAni EB (2 % w/w) in N-methylpyrrolidone (NMP) were prepared by stirring for *ca.* 48hrs. Solutions of PAni ES (2% w/w) in 3-Methylphenol ($CH_3C_6H_4(OH)$) were prepared by first dissolving the required quantity of PAni EB, then adding stoichiometric

quantities of HCS or H_2PP. It should be noted that PAni ES is weakly acidic, and a mean pK_a of 5.5 has been reported for ES titrated to EB in aqueous suspension. [33] Sulfonic acids are strongly monobasic, with $pK_a < 0$, and HCS will therefore efficiently protonate PAni EB producing PAni-CS. However, phosphorus oxyacids undergo a series of stepwise deprotonations, with each step exhibiting a progressively higher pK_a. For H_2PP the deprotonation equilibria are as follows. [34]

$$H_2PP_{(aq)} = HPP^-{}_{(aq)} + H^+{}_{(aq)} \quad pK_{a1} = 2.3 \tag{2}$$

$$HPP^-{}_{(aq)} = PP^{2-}{}_{(aq)} + H^+{}_{(aq)} \quad pK_{a2} = 7.8 \tag{3}$$

Thus, only the first pK_a is sufficiently acidic to efficiently protonate PAni EB and the resulting ES will be PAni-HPP.

The resulting mixtures were stirred for *ca.*168 hours and any (small) quantity of insoluble material was removed by centrifugation.

Solid films of PAni EB, PAni-CS and PAni-HPP were cast onto iron or glass substrates by pipetting the required quantity of solution onto the samples, which were subsequently levelled to ensure an even film thickness. The solvent was allowed to evaporate in air at 50°C.

The PAni films on iron were overcoated with a transparent layer of PVB to mechanically stabilize the ultrathin PAni layer. [28] This was done by bar casting a viscous ethanolic solution of PVB (15.5 % w/w) followed by air drying to produce a final PVB film thickness of (30 ± 5) μm, as determined using a micrometer screw gauge.

Electrical conductivity of PAni films was determined using four-point conductivity measurements in room air at 25°C. The PAni films for conductivity measurements were applied to glass microscope slides to produce a thickness of approximately (30 ± 5) µm. Four point gold electrode contacts were vapor deposited onto the PAni films using an Edwards vapor deposition apparatus under vacuum conditions.

Measurements of film thickness were either made directly using an atomic force microscope (AFM) or indirectly by measuring the optical absorbance of the PAni film. For direct measurements PAni ES films were scored and the depth of the resultant trough was measured directly using a Topmetrix Explorer atomic force microscope (AFM). Five measurements were taken in each case and averaged.

Indirect coating thickness measurements were carried out after corrosion driven coating delamination had occurred and all the PAni coating was in the EB form. The delaminated coating was mechanically removed, mounted on a glass microscope slide, and the UV-VIS absorbance spectrum recorded using a Perkin Elmer Lambda 1 spectrophotometer in transmission mode.

Film thickness (d) was calculated from the measured optical absorbance values using Equation 4 where $A_{\lambda max}$ is optical absorbance at the relevant spectral peak and $E_{\lambda max}$ is the extinction coefficient. Values of optical extinction coefficient for PAni ES and PAni EB were obtained by casting PAni ES films directly onto glass, measuring their thickness by AFM, then de-doping the films to PAni EB using 0.1 M aqueous NH_4OH. Absorbance spectra were obtained before and after de-doping, and an extinction coefficient for PAni EB and PAni ES calculated using Equation (4)

$$E_{\lambda max} = \frac{A_{\lambda max}}{d} \quad (4)$$

The methodologies for calibration of the SKP, obtaining the corrosion potential of polymer covered iron, and monitoring coating disbondment have been described elsewhere. [32] Reference solutions of 0.86 M aqueous NaCl were used to ensure a constant humidity of *ca*. 96 % RH within the SKP chamber. A temperature of 20 °C was maintained throughout.

The cathodic delamination of coatings was investigated using a 'Stratmann' type cell [15-17] whereby coatings were partially peeled back to create a defect comprising 10 mm x 10 mm of area of bare metal. A barrier between the intact coating and defect area was formed by the residual clear adhesive tape and PVB overcoating. The remaining sides of the defect were lined with non-corrosive silicone rubber in such a way that a 2 cm^3 volume of electrolyte could be applied to form a reservoir. Corrosion was initiated by applying an aliquot of 0.86 M aqueous NaCl to the coating defect. The SKP reference probe was scanned at a height of 100 µm along a 12 mm line normal to, and contiguous to, the defect coating boundary. The first scans were conducted immediately following the addition of the experimental electrolyte to the coating defect and successive scans were taken at 1 hour intervals thereafter.

It has previously been shown that the PAni state changes caused by the cathodic disbondment are visually recognizable in the case of transparent PAni ES layers applied to a carbon steel substrate. [31] Under normal oxygenated environmental conditions, the intact PAni ES appears green and the delaminated PAni EB appears blue. The cathodic delamination of PVB/PAni ES bilayer coatings could therefore be followed optically. Digital photographs were obtained in-situ at fifteen minute intervals using a Canon Power shot G6 digital camera with an external macro-lens. A Bayer filter system was used to

acquire red, green and blue pixel values. The red, green and blue filter pass bands were centered on 600 nm, 525 nm and 450 nm, respectively.

3. Results

3.1 Film thickness measurements

In all cases, the solution-cast PAni films were homogenous, flat, optically transparent and strongly adherent to the underlying substrate. There was no evidence of PAni precipitation or any other form of phase separation having occurred during solvent evaporation.

Figure 3 shows the UV-VIS absorption spectra obtained in the case of 0.07 μm thick films of PAni EB and PAni ES on glass. The spectra are entirely consistent with those reported elsewhere for PAni EB [35-37] and PAni ES. [3, 38] PAni EB exhibits two absorbance maxima, at *ca.* 325 nm and *ca.* 650 nm, which correspond to π-π* transition of the benzenoid ($[C_6H_4\text{-}NH]_m$) moiety and azaquinoid ($[C_6H_4\text{-}N{=}\ C_6H_4{=}N]_m$) group respectively. [36, 39] In the case of PAni ES absorbance maxima are observed at *ca.* 350 nm, *ca*. 410 nm.

(Figure 3)

Figure 4 shows the absorbance of PAni EB film at λ_{max} = 650 nm as a function of film thickness, as measured using AFM. The extinction coefficient (E_{650}), calculated from Figure 4 data using linear regression, was (2.12 ± 0.36) μm^{-1},which is similar to values of 3.2 μm^{-1} [40]and 16 μm^{-1} [41] reported elsewhere. Using a similar approach the extinction coefficient of PAni-CS at 325 nm, (E_{325}) was found to be (1.72 ± 0.23) μm^{-1}. This is similar to the value of 5.4 μm^{-1} recorded previously. [42] The value of E_{650} was routinely used to check the thickness of PAni films < 1 μm which had undergone cathodic disbondment. The value of E_{325} was not used quantitatively. However, the similarity of E_{325} with

published data from highly doped PAni ES films supports the notion that the PAni ES used here is also close to being stoichiometrically doped.

(Figure 4)

When PAni ES or PAni EB films were overcoated with 30 µm PVB layer to produce PVB/PAni bilayer coatings, there was no change in the UV-VIS absorption spectrum i.e. there was no optical indication of any reaction occurring between PAni and PVB.

3.2 Conductivity measurements

The lateral conductivity of PAni-CS solid films on glass was measured and found to be $(2.68 \pm 1.72) \times 10^{-2}$ $S.cm^{-1}$. The PVB/PAni ES dispersion coatings have electrical conductivities which are orders of magnitude lower than the solid films. A value of $(1 \pm 0.4) \times 10^{-4}$ $S.cm^{-1}$ was previously measured for 0.25 volume fraction of p-toluenesulfonic acid doped ES dispersed in PVB. [43] In the case of PVB/PAni ES dispersion coatings, for which PAni ES volume fractions were below 0.25, reliable conductivity values could not be obtained. The published range of conductivities for PAni ES is rather broad. For example, Yoshizawa et al. measured conductivities between 10^{-1} and 10^{-3} $S.cm^{-1}$ for PAni ES of MWT. 4500-6100 Da cast from NMP. [44] Similarly MacDiarmid et al. found conductivities of 10^{-2}-10^{-3} $S.cm^{-1}$ for PAni ES oligomers up to MWT. 3000 Da [45]. Thus the value of $(2.68 \pm 1.72) \times 10^{-2}$ $S.cm^{-1}$, reported in the case of the PAni-CS solid films here, falls within the reported range.

3.3 SKP Potentiometry

Initial studies were carried out to quantify the effect of PAni ES solid film thickness (*d*), upon the E_{corr} values measured in the absence of cathodic delamination. The significance

of E_{intact} in the context of polymer coated metal has been explained previously. [32, 46-47] In the case of non-conducting polymers, E_{intact} reflects the open circuit potential of the oxide-covered metal substrate, the value of which may be influenced by both Bronsted acid-base interactions, which occur between the polymer coating and oxide layer, and by reaction with atmospheric O_2. In the case of conducting polymers, electron transfer occurs between the substrate and the polymer layer, and E_{intact} will subsequently tend toward the redox potential (or Fermi level) of the conducting polymer. [12]

Time-dependent E_{intact} values obtained for PVB/PAni-CS and PVB/PAni-HPP bilayer coatings of various PAni ES thicknesses are shown in Figs 5a and 5b, respectively. The PAni coating weight corresponding to each PAni coating thickness was calculated using the known density of PAni EB (1.245 $g.cm^{-3}$). [48] In all cases the recorded E_{intact} values were substantially uniform over the sample surface, increasing slightly (< 0.1V vs. SHE) as a function of holding time throughout the first few hours within the SKP chamber. The change in E_{intact} with holding time in all cases is probably a result of water activity in the coating rising to come into equilibrium with the atmosphere (96 % RH) of the SKP chamber. [12] The constant (time-independent) value recorded thereafter implies that the PAni film is maintained in a substantially stable state. [12]

(Figure 5)

Figure 6 shows time-independent E_{intact} values (measured after 6 hours in the SKP chamber), for PVB/PAni EB and the various PVB/PAni ES bilayer coatings, plotted as a function of PAni ES layer thickness. Repeated E_{intact} measurements performed over unpigmented (plain) PVB coatings gave an E_{intact} value of (0.108 ± 0.018) V vs. SHE. In the case of PVB/PAni EB bilayer films, E_{intact} neither changes with PAni layer thickness, nor deviates

noticeably from that of the unpigmented PVB coatings (i.e. it remains ca. 0.108V *vs.* SHE). Conversely, for the PVB/PAni ES bilayer coatings, E_{intact} values increase with increasing PAni ES layer thickness for all layer thicknesses $< \sim 0.5$ μm but became constant thereafter, at which point E_{intact} values of 0.52 V vs. SHE and 0.4 V *vs.* SHE are recorded for the PAni-CS and PAni-HPP bilayer coatings. respectively.

(Figure 6)

3.4 Cathodic delamination of coatings

Delamination of unpigmented PVB coatings:- Initially, baseline delamination kinetics were obtained by following the corrosion-driven delamination of unpigmented PVB from a clean iron substrate. Numerous accounts of this system have been published previously. [15-17, 32] Following introduction of the corrosive electrolyte, time-dependent $E_{corr}(x)$ profiles became established within 240 minutes and examples are shown in Figure 7a. Figure 7a shows that in the intact (undelaminated) region of the sample the potential (E_{intact}) remains uniformly high at a constant value of *ca.* 0.10 V vs. SHE. Conversely, potential (E_{corr}) values recorded near the coating defect fall to that expected of freely corroding iron (*ca.* -0.44 V vs. SHE), both these values being consistent with measurements made previously. [15-17] Loss of coating adhesion is believed to be a result of OH^- or reactive intermediates produced by the COR, attacking the coating/substrate bond at the delamination front. [15] Anodic activity takes place in the defect and the two regions are linked by the flow of ionic current in the film of electrolyte drawn under the delaminated coating. [15] The sharp inflection in potential seen moving from left to right in Figure 7a as time increases can used as a semi-empirical indication of the position of the delamination front. [15, 32, 49]

On the basis of the above, the time-dependent distance from the coating defect to the delamination front (x_{del}) may be obtained by locating the point of highest potential gradient in the relevant E_{corr} profiles delamination profiles shown in Figure 7. [15] By plotting x_{del} as a function of the associated delamination time, t_{del}, it is possible to study the kinetics of coating delamination. In the case of uninhibited coatings, delamination rates are typically controlled by the migration of electrolyte cations (here Na^+) beneath the delaminated coating. [15-16] Under these conditions delamination kinetics are predicted to be parabolic and to follow Equation 5, where t_i is the time taken for corrosion-driven delamination to become initiated and k_d is the parabolic delamination rate constant.

$$x_{del} = k_d(t_{del} - t_i)^{\frac{1}{2}} \quad (5)$$

The first curve in both Figure 8a and Figure 8b shows x_{del} plotted as a function of t_{del}-t_i for the unpigmented PVB coating and the k_d value obtained by analyzing this data according to Equation 5 was (334 ± 48) µm.min$^{-1/2}$.

(Figure 7)

(Figure 8)

Delamination of PVB/PAni EB bilayer coatings: - The typical E_{corr} profiles obtained in the case of a PVB/PAni EB bilayer coating is shown in Figure 7b. Comparison of Figure 7a and Figure 7b indicates that the presence of a PAni EB layer does not significantly change the E_{corr} profiles from those observed for unpigmented PVB. This finding is consistent with previous results obtained using PVB/PAni EB dispersion coatings. [12] Parabolic kinetics, consistent with cation migration control, are again observed for the delamination of the PVB/PAni EB bilayer coatings. A parabolic rate constant of (194 ± 57) µm.min$^{-1/2}$ was

obtained by fitting x_{del} *vs* (t_{del} $-t_i$) data to Equation 5. This value is similar, within experimental error, to that observed in the case of unpigmented PVB.

Delamination of PVB/PAni ES bilayer coatings: - The E_{intact} values obtained in the case of both PVB/PAni-CS and PVB/PAni-HPP bilayer coatings were ennobled when compared to unpigmented PVB coatings. Figure 7c shows a typical example of the time-dependent E_{corr} profiles obtained in the case of a PVB/PAni-CS bilayer coating with a PAni-CS layer thickness 0.031 μm. Similar behavior can be seen in Figure 7d for a PVB/PAni-HPP bilayer coating with a PAni-HPP thickness 0.033 μm. Delamination kinetics were also modified relative to unpigmented PVB.

Figure 8a and Figure 8b show plots of x_{del} as a function of (t_{del}-t_i) obtained from various PVB/PAni ES bilayer coatings. For coating thicknesses of up to 0.44 μm in the case of PVB/PAni-CS, and 0.49 μm in the case of PVB/PAni-HPP, predominately parabolic kinetics consistent with Na^+ migration control, are observed. [15] In the case of higher thicknesses, under-film Na^+ cation migration ceases to be the rate determining process, and linear kinetics are observed. The value at which this change occurs coincides approximately with the PAni ES layer thickness at which E_{intact} values became constant in Figure 6.

3.5 Optical cathodic disbondment data: - It has previously been shown that the PAni state changes caused by the cathodic disbondment are visually recognizable in the case of transparent PAni ES layers applied to a carbon steel substrate. [31] Under normal oxygenated environmental conditions, the intact PAni ES appears green, and PAni LB appears colourless. In the work reported here PAni state changes were only found to be visible in this way for solid PAni films < *ca.*1μm thick. For film thicknesses > 1μm, the PAni was

too optically absorbent for ready interrogation using the equipment available (digital photography). For this reason, all optical studies were carried out using thin (~0.30μm) PAni ES layers overcoated with clear PVB (30 μm).

Cathodic delamination of the PVB/PAni ES bilayer coating was monitored by using a combination of time lapse photography and SKP potentiometry, the results being shown in Figure 9. A typical SKP E_{corr} profile obtained for the delamination of the PVB/PAni-CS bilayer coatings from iron is shown in Figure 9a. The corresponding image of the delaminating coating is shown in Figure 9b. The Bayer filter system used to acquire the red, green and blue pixel values had red, green and blue filter pass bands centered on 600 nm, 525 nm and 450 nm respectively. Although a filter pass band width does not permit a fully quantitative analysis of spectrum, a semi-quantitative analysis is possible in terms of the concentrations of ES, LS and EB and is shown in Figure 9c.

The colors visible in Figure 9b arise from the absorbance of light passing through the PAni coating layer before, and after, reflection from the iron substrate. To analyze the data, red, green and blue pixel values were acquired over eight lines normal to the delamination front. Optical absorbance values were then calculated using Equation 6 and Equation 7, where quantity I denotes the digital light intensity value (between 0 and 255) associated with a particular green or blue pixel. I_{max} denotes the maximum light intensity associated with green or blue pixels anywhere in the image, including areas where PAni is in the non-absorbing LS so that I_{max} is a measure of light transmitted in the absence of PAni absorption (I_0 in standard Beer-Lambert notation).

$$A_{Green} = -\log_{10}\left[\frac{I_{Green\ pixel}}{I_{\max Green\ pixel}}\right] \quad (6)$$

$$A_{Blue} = -\log_{10}\left[\frac{I_{Blue\ pixel}}{I_{\max Blue\ pixel}}\right] \quad (7)$$

By reference to Figure 9, the quantity A_{Green} corresponds reasonably well to absorbance by PAni EB such that we may write

$$[EB] = c_1.A_{Green} \quad (8)$$

$$[EB]_N = \frac{[EB]}{[EB]_{max}} \quad (9)$$

where *c* is a constant and *[EB]* is the concentration of emeraldine base in the PAni film, $[EB]_{max}$ is the maximum *[EB]* value in the image file and $[EB]_{norm}$ is the normalized *[EB]* value. Because $[EB]_{max}$ derives from portions of the image that are known to contain only EB, the quantity $[EB]_N$ corresponds to the fraction of total PAni in the EB state. We can similarly write

$$[ES] = c_2.A_{Blue} \quad (10)$$

$$[ES]_N = \frac{[EB]}{[EB]_{max}} \quad (11)$$

where *[ES]* is the concentration of emeraldine salt in the PAni film, $[ES]_{max}$ is the maximum *[ES]* value in the image file and $[ES]_N$ is the normalized *[ES]* value. By an extension of this reasoning we can write equation (10) where $[LB]_N$ is the amount of PAni in the leuco state.

$$[LB]_N = 1 - ([ES]_N + [EB]_N) \quad (12)$$

Equation 6 to Equation 12 worked well in all parts of the image where only ES and LB were present but the blue filter pass band width rendered these inaccurate due to the presence of EB in areas in which the coating had fully delaminated (blue). The $[ES]_N$ value

is adjusted to Equation 13 in the delaminated region because of the absorbance overlap in the blue.

$$[ES]_N = 1 - [EB]_N \quad (13)$$

Figure 9c thus shows the normalised concentration of the PAni states present, analysed in terms of colour intensity of the individual pixels from the image shown in Figure 9b. A high uniform potential of ca. 0.25 V vs. SHE (Figure 9a), consistent with an intact coating, corresponds to region in which green PAni ES is observed. In the region of the delamination front the coating becomes transparent, this being indicative of the reduction of PAni ES to PAni LB. The low E_{corr} values observed in the delaminated region coincides with the presence of blue PAni EB, which indicates the delaminated region of coating. The exact point at which coating delamination occurs is assumed to be where the normalised concentration of PAni EB begins to rise from the minimum value, i.e. at approximately 7800 µm from the defect. It can thus be seen that PAni LB is re-oxidised to PAni EB in the delaminated region.

(Figure 9)

Knowing the point at which coating delamination occurs, and the rate of coating disbondment, it is possible to calculate the time that lapses before coating re-oxidation. Figure 10 shows $[EB]_N$ as a function of time, from which it can clearly be seen that re-oxidation of 80 % of the 0.30 µm PAni LB coating to PAni EB takes approximately 30 minutes.

(Figure 10)

The kinetics obtained from Figure 10 (in the case that PAni LB, freshly delaminated from an iron surface, was re-oxidised to PAni EB) were compared to those obtained in the case that PAni LB was allowed to re-oxidise to PAni EB in isolation, under atmospheric conditions. Films of PAni-CS of thickness 0.20 μm, were applied to ITO coated glass and were reduced to PAni LB by applying a potential of -0.2 V vs. SCE in 0.86 M aqueous NaCl. Subsequently 1 ml of 0.1 M ammonium hydroxide was added to the electrolyte to ensure full de-protonation of the resulting PAni LS to PAni LB. The colourless PAni film was mounted in the UV-VIS spectrophotometer and the optical absorbance of the film recorded at the peak absorbance of the quinoid segment of the polymer obtained from Figure 3 (650 nm).

As can be seen in Figure 11, the absorbance recorded had not reached the value of ~0.4 expected for PAni EB even after 400 hours of atmospheric exposure and therefore, a large difference exists between the re-oxidation kinetics obtained in the case of a PAni film delaminating from an iron substrate the case of an isolated PAni film. It appears therefore that the presence of iron ions acts to catalyse the PAni LB re-oxidation reaction. The mechanism of PAni ES induced interfacial oxide growth has been characterized elsewhere and is shown in Figure 2. [32] Fe^{2+} cations released during the oxidation of Fe exist as a dynamically established Fe^{2+} dopant salt concentration. The notion of Fe catalysis is consistent with previous work which has shown that the presence of $FeCl_3$ reduces the re-oxidation time of PAni LB to PAni EB to a few minutes, compared with several hours for atmospheric re-oxidation in the absence of $FeCl_3$. [37]

(Figure 11)

It is important to note that PAni-HPP exhibits an optical behavior which is significantly different from that of PAni-CS. Figure 12 shows larger format digital images obtained from (a) an actively delaminating PVB/PAni-CS bilayer coating and (b) an actively delaminating PVB/PAni-HPP bilayer coating. Comparing the two images shows that whilst PAni-CS exhibits a distinct region of PAni LB (a leuco band), no such leuco band is apparent in the case of PAni-HPP. These findings are immediately consistent with PAni-CS becoming exhaustively reduced by cathodic electron transfer to iron at the coating delamination front. However, there is no indication that PAni-HPP is subject to a similar exhaustive reduction. Conversely, it appears that PAni-HPP becomes directly converted to PAni EB without going through the leuco state. It is also noteworthy that the mottled blue/green coloration in the intact (undelaminated) portion of Figure 12b is consistent with a partial de-doping (conversion to PAni EB) of the PAni-HPP layer.

(Figure 12)

4.0 Discussion

4.1 Comparison of PVB/PAni EB bilayer and PVB/PAni EB dispersion coatings

In the case of electrically nonconducting PVB/PAni EB bilayer films, E_{intact} values are completely independent of PAni EB thickness (coating weight) and remain similar to E_{intact} measured over unpigmented PVB coatings (Figure 6). This is consistent with previous work during which E_{intact} values, measured over PVB coatings in which PAni EB was dispersed, were found to be independent of PAni fraction. [12] As previously discussed, in the case of non-conducting polymers, E_{intact} reflects the open circuit potential of the oxide-covered metal substrate, the value of which may be influenced by both Bronsted acid-base interactions, which occur between the polymer coating and oxide layer, and by reaction

with atmospheric O_2. The findings for both PVB/PAni EB bilayer and PVB/PAni EB dispersion coatings are therefore consistent with the notion that electron transfer does not occur between the iron substrate and solid PAni EB film to any significant degree.

With regards to the kinetics of corrosion-driven coating delamination, the use of PVB/PAni EB bilayer coatings is found to have little effect, and E_{corr} profiles do not deviate from those obtained in the case of unpigmented PVB. Parabolic kinetics, consistent with electrolyte Na^+ migration control is observed in both cases. There is no evidence that the PAni EB solid films act to influence Na^+ mobility or coating adhesion or by buffering under film pH, [12, 32] all of which have an effect on delamination rate. [12, 16, 32] Previously it has been found that the PAni EB dispersed within PVB similarly has no effect on delamination kinetics, regardless of coating pigment loading, [12] and it is therefore proposed that PAni EB is electrochemically inert and ineffective in preventing the corrosion-driven cathodic disbondment of coatings, regardless of phase continuity. It has previously been claimed that PAni EB provides corrosion protection and that doping is unnecessary. [50-57] However, in the case of the PVB/PAni EB bilayer coating, this does not seem to be correct.

4.2 Comparison of PVB/PAni ES bilayer films and PVB/PAni ES dispersion coatings

Unlike the PAni EB case, the PVB/PAni ES bilayer coatings exhibit E_{intact} values which tend towards the dopant dependent redox potential of the PAni ES at coating thicknesses ≥ 0.5 μm. The relevant E_{intact} values were recorded as 0.51 V vs. SHE and 0.38 V vs. SHE for PAni-CS and PAni-HPP, respectively (Figure 6). However, at PAni ES layer thickness < 0.5 μm, E_{intact} decreases with layer thickness and tends toward the PAni EB E_{intact} value (~ 0.1 V vs. SHE) as layer thickness tends towards zero. One possible explanation for this phenomenon is that layer discontinuity (e.g. pinholes) becomes more significant as layer

thickness decreases. However, there was no visible evidence that this was the case and it seems reasonable to propose that the drop in potential results from a partial de-doping of the PAni ES. In the case of PAni-HPP, de-doping would arise as a straightforward consequence of interfacial salt formation, Equation 14.

$$Fe + 2(PAniHPP) \rightarrow Fe(HPP)_2 + 2(PAniEB) \quad (14)$$

Such a process is immediately consistent with the bluish mottling observed for a PAni-HPP layer in Figure 12b. In the case of PAni-CS, the mechanism of partial de-doping is less clear but could arise from the dynamic establishment of an iron-CSA salt concentration as part of the interfacial oxide growth mechanism (Figure 2). In both cases, the quantity of iron dopant salt formed would be finite and reach a constant (limiting) value as PAni ES layer thickness increases. One implication of such a proposal is that, in the case of the PAni-HPP bilayer coating, the interfacial salt film becomes fully formed (of self-limiting thickness) for PAni-HPP layer thickness ≥ 0.5 μm.

The results described above are similar to those obtained in the case of PVB/PAni ES dispersion coatings. [12] For the dispersion coatings, E_{intact} was found to increase with PAni ES volume fraction up to a volume fraction of 0.25, at which point steady state E_{intact} values of 0.42 V vs. SHE and 0.43 V vs. SHE were observed in the case of PAni-HPP and PAni-CS respectively. [12] However, the physical cause is probably different. In the case of the dispersion coatings, the metal/coating interface is non-uniform and composed of a mosaic of PVB/iron and PAni ES/iron areas (Figure 13a). Thus, as PAni ES volume fraction increases, so will the fractional area contribution of the PAni ES/iron interface.

(Figure 13)

With regards to the kinetics of corrosion-driven coating delamination, delamination rate was found to be strongly dependent on the quantity of PAni ES present and the identity of the dopant anion for both bilayer and dispersion coatings. To allow a direct comparison between bilayer and dispersion coatings it is convenient to express the quantity of PAni ES present as a coating weight. In the case of dispersion coatings, values of PAni ES volume fraction and total coating thickness (30 μm) were used to calculate a corresponding solid PAni coating weight. In the case of bilayer coatings, the coating weight was calculated directly from the coating thickness. In all calculations the PAni density was taken to be the published density for PAni EB, 1.245 $g.cm^{-3}$. [48]

Because the observed delamination kinetics change from parabolic to linear as PAni ES layer thickness increases, the initial rate of coating delamination was used for purposes of comparison. Initial rates were estimated by construction of a tangent to the x_{del} vs. $(t_{del} - t_i)$ curves at $(t_{del} - t_i) = zero$. Figure 14 shows the reciprocal of the initial rate of cathodic disbondment as a function of coating weight for a.) PVB/PAni-CS bilayer coatings and PVB/PAni-CS dispersion coatings and b.) PVB/PAni-HPP bilayer coatings and PVB/PAni-HPP dispersion coatings. At low PAni ES coating weights (< 0.05 mg cm^{-2}), the delamination rate was found to be inversely proportional to coating weight and to be significantly slower in the case of the continuous (bilayer) coatings when compared with the corresponding (same PAni ES) dispersion coating. In the case of PAni-CS (Figure 14a), the same was also observed for coating weights > 0.05 mg cm^{-2}. However, in the case of PAni-HPP solid films of coating weights > 0.05 mg cm^{-2}, the delamination rate became independent of coating weight. Figure 14b also shows that for PAni ES coating weights ~ 0.12 mg cm^{-2}, the PVB/PANi-HPP bilayer coatings delaminate faster than the corresponding dispersion coatings.

Any mechanistic rationalization of the complex results shown above will necessarily have a speculative component. Nevertheless, they can be explained, at least in part, by considering the nature of the coating/iron interface. In the case of the dispersion coatings, the interface will be a mosaic of PVB/metal and PAni ES/metal areas, as shown schematically in Figure 13a. In order for coating delamination to occur, the PVB/metal bond must therefore be broken, a process which occurs as a result of the OH^- or reactive intermediates of the COR (Equation 15) being released at the PVB/metal interface. [15] However, the promotion of E_{intact} (Figure 6) by PAni ES may act to suppress the COR at the PVB/metal interface. In so doing the PAni ES will become 'sacrificially' reduced to PAni LB via Equation 16. Suppression of Reaction 15 will only cease once all the PAni ES in electrical contact with the iron surfaces has been reduced to the leuco state (although it may become re-oxidized to inactive EB in the delaminated coating).

$$O_2 + 2H_2O + 4e^- \rightarrow 4OH^- \quad (15)$$

$$PAni^+A^-(ES) + e^+ \leftrightharpoons PAni(LB) + A^- \quad (16)$$

Under these circumstances the time taken for successive portions of the coating to delaminate will be roughly proportional to the PAni ES coating weight, implying that the delamination rate will be inversely proportional to the PAni ES coating weight. Such a predication is immediately consistent with the linear nature of the reciprocal rate plots for PAni-CS and PAni-HPP dispersion coatings shown in Figure 14. The observation that PVB/Pani-HPP dispersion coatings delaminate more slowly than PVB/PAni-CS dispersions of the same PAni ES coating weight can be explained by the relative influence on interfacial electron transfer rate of the PAni-HPP/iron interfacial salt film and the PAni-CS/iron interfacial oxide film. [12]

In contradistinction to the above, the interface between iron and the PAni ES solid films of the bilayer coatings will be uniform and continuous, as shown schematically in Figure 13b. Consequently, there is no PVB/iron interface, and coating delamination requires only the failure of the PAni ES/iron bond. Under these circumstances, delamination kinetics will be determined mainly by the nature of the interphase developing between PAni ES and iron. [12] In the case of PAni-CS this interphase will comprise of iron oxide, [12] which is only very weakly amphoteric, and therefore stable at the high pH values (as high as pH 14) associated with cathodic coating delamination on iron. [15] In the case of PAni-HPP it will consist of an iron HPP^- salt film. [12] The second pK_a of phenyl phosphonic acid is 7.8, which implies that the HPP- anions of the salt film will deprotonate under conditions of cathodic disbondment. [15] The resulting mixed iron/sodium PP^{2-} salt is likely to exhibit significant water solubility.

On the basis of the above, it proposed that in the case of the PVB/PAni-CS bilayer coatings the PAni-CS/iron interphase is resistant to chemical dissolution by the alkaline (NaOH) underfilm catholyte and coating delamination only occurs once all the PAni-CS has been exhaustively electrochemically reduced and COR commences on the PAni-iron interphase. This notion is consistent with the appearance of a leuco band (PAni LB) in Figure 9b and Figure 10a. It is also consistent with the linearity of the reciprocal rate plot in Figure 14a.

Contrary to in the case of the PVB/PAni-HPP bilayer coatings, the PAni-HPP/iron interphase is susceptible to chemical dissolution by the alkaline catholyte which develops beneath the delaminated coating. (Note the COR can occur on iron anywhere under the delaminated coating and not just at the delamination front where it may be suppressed by PAni ES.) In this case the PAni-HPP layer would become chemically disbonded from the iron substrate, electrical contact between PAni ES and iron would be lost, and iron ES electron transfer would cease. Under these circumstances an exhaustive electrochemical

reduction of PAni ES might not occur before coating delamination took place. This notion is consistent with the absence of a leuco band (PAni LB) in Figure 12b. It is also consistent with invariance of coating delamination rate with PAni-HPP coating weight for coating weights > 0.05 $mg.cm^{-2}$ (Figure 14b).

(Figure 14)

On the basis of the above, it would seem that the continuity (or not) of the PAni ES influences resistance to delamination chiefly by determining the continuity (or not) of the interphase which develops at points of contact between PAni ES and the underlying iron substrate (at least when that interphase is susceptible to chemical attack by the underfilm catholyte). However, there is also evidence that the in-coating continuity of the PAni ES can play a role directly. Comparison of the reciprocal delamination rate data for PVB/PAni-CS bilayer coatings and dispersion coatings in Figure 14 shows that, for any given PAni-CS coating weight, the bilayer coatings delaminate more slowly than the dispersion coatings. This could be explained on the basis of the higher through-film electronic charge percolation of the PAni-CS solid layer, allowing a higher fraction (potentially all) of the PAni-CS to sacrificially suppress the COR. Conversely, the relatively poor through-film charge percolation of the dispersion coating would result in PAni-CS particles in the outer part of the coating (farthest from the iron surface) becoming electrically isolated from iron as PAni-CS reduction proceeds. Under these circumstances the fraction of PAni-CS available to suppress the COR in PVB/PAni-CS dispersion coatings would be < 1.

5. Conclusions

A systematic electrochemical electrochemical and optical study has been carried out into how the quantity and phase continuity of PAni ES, present within an organic coating,

affects the rate at which that coating undergoes corrosion-driven cathodic delamination. In so doing, PAni ES dispersion coatings comprising of a PAni ES powder dispersion in electrically non-conductive PVB have been compared with PVB/PAni ES bilayer coatings. Furthermore, sulfonic acid doped PAni-CS has been compared with phosphonic acid doped PAni-HPP. The complex results have been explained on the basis of a series of hypothesis which can be summarized as follows:

1. For PAni-CS, the interphase which forms at points of PAni ES/iron contact is an insoluble oxide, but for PAni-HPP it is a weakly acidic salt film (which is likely to react with, and become dissolved by, chemical reaction with underfilm aqueous NaOH produced through the COR).

2. For the PVB/PAni ES dispersion coatings, the interphase which forms with iron is discontinuous, so that its chemical dissolution cannot produce coating disbondment. Conversely, for the bilayer coatings the interphase is continuous and chemical dissolution of the interphase can produce coating disbondment.

On the basis of the above the following predictions can be made:

1. For both the PVB/PAni-CS and PVB/PAni-HPP dispersion coatings, disbondment will only occur once the COR becomes established at the iron/PVB interface. This can only happen after all the local PAni-ES has been electrochemically reduced (because PAni ES is a cathodic depolarizer and sacrificially suppresses the COR).

2. For the PVB/PAni-CS bilayer, coating disbondment will only occur once the COR becomes established at the PAni-CSA/iron interface. This can only happen after all the local PAni-CSA has been electrochemically reduced (for the same reason as above).

3. For the PVB/PAni-HPP bilayer coating, disbondment can occur without the COR becoming established at the PAni-HPP/iron interface. This can happen because NaOH produced under the already delaminated coating (by through-coating COR taking place in the delaminated region not at the disbondment front) can chemically react with and dissolve the weakly acidic iron/HPP salt film interphase.

4. In all cases, PAni ES will end up as PAni EB in the delaminated region. Either through electrochemical reduction and atmospheric re-oxidation (in the case of the dispersion and bilayer PVB/PAni-CS coatings and the PVB/PAni-HPP dispersion coating) or by direct chemical de-doping through an acid-base reaction (in the case of the PVB/PAni-HPP bilayer coating).

These predictions are borne out experimentally and lead to further implications:

1. Long range charge percolation within the PAni ES phase is not necessarily injurious to delamination resistance. The PVB/PAni-CS bilayer coatings delaminate more slowly than PVB/PAni-CS dispersion coatings with similar PAni-CS coating weight, presumably because the higher electrical conductivity of the PAni-CS solid film makes a larger fraction of the in-coating PAni-CS available to sacrificially suppress the COR and because of the electrical resistance of the relatively thick oxide layer which grows beneath the PAni-CS coating. This means that continuous PAni-ES coatings might not necessarily lead to weak delamination resistance as long as the electron transfer across the interface is sufficiently (but not fully) inhibited.

2.Continuity (or not) of the PAni ES phase chiefly influences coating delamination resistance by determining the continuity (or not) of the PAni ES/iron interphase. However, this is only significant if the chemical behavior of that interface in the alkaline underfilm

607 catholyte is significantly different to that of the PVB/iron interface (i.e. it is susceptive to
608 attack through an acid-base reaction).

609 5. Acknowledgments

610 The authors would like to thank EPSRC and Tata Steel UK for funding this work.

611 6. Figure Legends

612 Figure 1. Redox and acid base equilibria in polyaniline. The number of protons and
613 electrons shown are for every two aniline residues. Reproduced with permission.[12]

614 Figure 2. The mechanism of of PAni-pTS induced oxide growth on iron at 93 % RH.
615 Reproduced with permission. [32]

616 Figure 3. UV-VIS absorption spectra for 0.07 µm thick homogeneous solid PAni EB and
617 PAni ES films. λ_{max} PAni ES = 410nm, λ_{max} PAni EB = 650nm.

618 Figure 4. Absorbance as a function of PAni EB solid film thickness. Each value is taken at
619 λ_{max}= 650 nm.

620 Figure 5. SKP derived E_{intact} for homogenous a.) PVB/PAni-CS and b.) PVB/PAni-HPP
621 bilayer coatings of varying PAni ES thickness (coating weight), on an iron substrate as a
622 function of time. Measurement were taken in air at 96 % R.H. and 20 ˚C. The equivalent
623 coating weight was calculated using the known density of PAni EB.

624 Figure 6. SKP derived E_{intact} for homogeneous PVB/PAni EB (●), PVB/PAni-CS (▲) and
625 PVB/PAni-HPP bilayer coatings of varying PAni thickness (coating weight), on an iron
626 substrate. Measurements were taken after six hours of the samples being placed in the SKP
627 in air at 96 % R.H. and 20°C.

628 Figure 7. SKP derived E_{corr} as a function of distance from defect *(x)* profiles for a.) 30 µm
629 PVB coating on an iron substrate, b.) 0.25 µm PAni EB solid film over coated with 30µm
630 PVB, c.) 0.31 µm PAni-CS solid film over coated with 30µm PVB d.) 0.33 µm PAni-HPP
631 solid film over coated with 30µm PVB. Key: (*) 240 min after initiation with 0.86 M NaCl
632 and 120 (a, c, d) and 180 (b) minute intervals thereafter.

633 Figure 8. Plots of delamination distance (x_{del}) vs. time for homogenous a.) PVB/PAni-CS
634 and b.) PVB/PAni-HPP bilayer coatings of varying PAni-ES thickness (coating weights).
635 Measurements were taken in air at 96 % R.H. and 20˚C.

636 Figure 9. a.) SKP derived E_{corr} as a function of distance from defect *(x)* profiles for the
637 delamination of a PVB/PAni-CS bilayer coating, from an iron substrate after initiation
638 using a 0.86 M NaCl electrolyte, b.) Digital image of the sample surface and c.) the
639 normalised concentration of the PAni states present, analysed in terms of colour intensity

of the individual pixels from the image shown in Figure 8b. All data was recorded 12 hours after initiation.

Figure 10. PAni-CS re-oxidation kinetics showing the time taken for the colourless PAni LB (adhered to an iron substrate) to fully reoxidise to the blue PAni EB after delamination has occurred.

Figure 11. PAni-CS re-oxidation kinetics showing the time taken for the colourless 0.20 μm PAni LB, adhered to an ITO coated glass, to fully re-oxidise to blue PAni EB under atmospheric conditions.

Figure 12. Digital image of the sample surface during the delamination of a.) a PVB/PAni-CS bilayer coating and b.) a PVB/PAni-HPP bilayer coating, from an iron substrate, after initiation using a 0.86 M NaCl electrolyte.

Figure 13. Schematic showing the continuity of the coating/iron interface in the case of PVB/PAni-ES a.) dispersion and b.) bilayer coatings. In the case of PAni-CS the PAni-ES/iron interphase will consist of an insoluble oxide and in the case of PAni-HPP it will consist of a soluble salt film.

Figure 14. Reciprocal delamination rate as a function of ES coating weight (thickness) comparing PVB/PAni-ES bilayer coatings with PVB/PAni-ES dispersion coatings in the case that the dopant of interest is a.) HCS and b.) H_2PP. The equivalent coating weight was calculated using the known density of PAni EB.

7. References

1. D. Tallman, G. Spinks, A. Dominis, G. Wallace, *Journal of Solid State Electrochemistry*, 6, 73 (2002).
2. G. Spinks, A. Dominis, G. Wallace, D. Tallman, *Journal of Solid State Electrochemistry*, 6, 85 (2002).
3. B. Wessling, *Synthetic Metals*, 85, 1313 (1997).
4. B. Wessling, *Advanced Materials*, 6 (1994).
5. N.Y. Abu-Thabit, A.S.H. Makhlouf, in: Handbook of Smart Coatings for Materials Protection, A. S. H. Makhlouf, Editor, p. 459, Woodhead Publishing (2014).
6. N. Pirhady Tavandashti, M. Ghorbani, A. Shojaei, J.M.C. Mol, H. Terryn, K. Baert, Y. Gonzalez-Garcia, *Corrosion Science*, 112, 138 (2016).
7. M. Rohwerder, L.M. Duc, A. Michalik, *Electrochimica Acta*, 54, 6075 (2009).
8. M. Rohwerder, S. Isik-Uppenkamp, C.A. Amarnath, *Electrochimica Acta*, 56, 1889 (2011).

9. Y. Zhang, Y. Shao, X. Liu, C. Shi, Y. Wang, G. Meng, X. Zeng, Y. Yang, *Progress in Organic Coatings*, 111, 240 (2017).

10. R. M. Bandeira, J. van Drunen, G. Tremiliosi-Filho, J. Ribeiro dos Santos, J. M. Elias de Matos, *Progress in Organic Coatings*, 106, 50 (2017).

11. M. Kohl, A. Kalendová, *Progress in Organic Coatings*, 86, 96 (2015).

12. G. Williams, A. Gabriel, A. Cook, H.N.McMurray, *Journal of the Electrochemical Society*, 153, B425 (2006).

13. B. Wessling, *Synthetic Metals*, 102, 1396 (1999).

14. H. Leidheiser, W. Wang, in *Corrosion Control by Organic Coatings*, H. Leidhesier, Editor, p.70, NACE, Houston (1981)

15. A. Leng, H. Streckel, M. Stratmann, *Corrosion Science*, 41, 547 (1999).

16. A. Leng, H. Streckel, M. Stratmann. *Corrosion Science*,41, 579 (1999).

17. M. Stratmann, R. Feser, A. Leng, *Electrochimica Acta*, 39, 1207 (1994).

18. M. C. Bernard, S. Joiret, A. H.-Le Goff, P. V. Phong, *Journal of the Electrochemical Society*, 148, B12 (2001).

19. P. J. Kinlen, V. Menon, Y. Ding, *Journal of the Electrochemical Society*, 146, 3690 (1999).

20. P. J. Kinlen, Y. Ding, D. C. Silverman, *Corrosion*, 58, 490 (2002).

21. T. K. Rout, G. Jha, A. K. Singh, N. Bandyopadhyay, O. N. Mohanty, *Surface and Coatings Technology*, 167, 16 (2003).

22. X. Lu, H. Y. Ng, J. Xu, C. He, *Synthetic Metals*, 128, 167 (2003).

23. J. Yano, M. Kobayashi, S. Yamasaki, Y. Harima, K. Yamashita, *Synthetic Metals*, 119, 315 (2001).

24. W. Lu, R. L. Eisenbaumer, B. Wessling, *Synthetic Metals*, 71, 2163 (1995).

25. S. Tawde, D. Mukesh, and J. V. Yakhmi, *Synthetic Metals*, 125, 401 (2002).

26. P. J. Kinlen, Y. Ding, D. C. Silverman, *Synthetic Metals*, 85, 1327 (1997).

27. M. Kendig, M. Hon, L. Warren, *Progress in Organic Coatings*, 47, 183 (2003).

28. M. Rohwerder, A. Michalik, *Electrochimica Acta*, 53, 1300 (2007).

29. A. Michalik, M. Rohwerder, *Zeitschrift fur Physikalische Chemie*, 219,1547 (2005).

30. G. Paliwoda-Porebska, M. Rohwerder, M. Stratmann, U. Rammelt, L. M. Duc, W. Plieth, *Journal of Solid State Electrochemistry*, 10, 730 (2006).

31. A. Gabriel, A. N. J. Laycock, H. N. McMurray, G. Williams, A. Cook, *Electrochemical and Solid State Letters*, 9, B57 (2006).

32. R. J. Holness, G. Williams, D. A. Worsley, H. N. McMurray, *Journal of the Electrochemical Society*, 152, B73 (2005).

33. C. Menardo, M. Nechtschein, A. Rousseau, J. P. Travers, P. Hany, *Synthetic Metals*, 25, 311 (1988).

34. L. D. Freedman, G. O. Doak, *Chem. Rev. (Washington, D.C.)*, 57, 479 (1957).

35. Y. Y. Wang, X.L. Jing, *Polymer Testing*, 24, 153 (2005).

36. M. X. Wan, *Journal of Polymer Science Part A-Polymer Chemistry*, 30, 543 (1992).

37. D. K. Moon, M. Ezuka, T. Maruyama, K. Osakada, T. Yamamoto, *Macromolecules*, 26, 364 (1993).

38. L. A. P. Kane-Maguire, A. G. MacDiarmidb, I. D. Norrisa, G. G. Wallace, W. Zheng, *Synthetic Metals*, 106, 171 (1999).

39. J. M. Wilbur, T. C. Sandreczki, I. M. Brown, D. J. Leopold, S. Mohite, *Synthetic Metals*, 82, 175 (1996).

40. J. A. Osaheni, S. A. Jenekhe, H. Vanherzeele, J. S. Meth, Y. Sun, A. G. MacDiarmid, *J. Phys. Chem.*, 96, 2830 (1992).

41. F. Fitrilawati, M. O. Tjia, *Optical Materials*, 16, 361 (2001).

42. J. Stejskal, I. Supurina, J. Prokeš, J. Zemek, *Synthetic Metals*, 105, 195 (1999).

43. G. Williams, H. N. McMurray, *Electrochemical and Solid-State Letters*, 8, B42 (2005).

44. A. Yoshizawa, M. Takeda, Y. Oura, Y. Takemoto, K. Naoi, *Electrochemistry*, 67, 45 (1999).

45. A. G. MacDiarmid, Y. Zhou, J. Feng, *Synthetic Metals*, 100, 131 (1999).

46. A. Leng, A, H. Streckel, K. Hoffman, M. Stratmann, *Corrosion Science*, 41, 599 (1998).

47. A. P. Nazarov, D. Thierry, *Protection of Metals*, 39, 55 (2003).

48. J. Stejskal, R. G. Gilbert, *Pure and Applied Chemistry*, 74, 857 (2002).

49. G. Williams, G., H. N. McMurray, *Journal of the Electrochemical Society*, 148, B377 (2001).

734 50. M. Fahlman, S. Jasty, A. J. Epstein, *Synthetic Metals*, 85, 1323 (1997).

735 51. A. Talo, O. Forsen, A.Yläsaari, *Synthetic Metals*, 102, 1394 (1999).

736 52. A. Mirmohseni, A. Oladegaragoze, *Synthetic Metals*, 114, 105 (2000).

737 53. A. J. Dominis, G. M. Spinks, G. G. Wallace, *Progress in Organic Coatings*, 48, 43
738 (2003).

739 54. G. M. Spinks, A. J. Dominis, G. G. Wallace, *Corrosion*, 59, 22 (2003).

740 55. Y. Y. Wang, X. L. Jing, *Polymer Journal*, 36, 374 (2004).

741 56. A. M. Fenelon, C. B. Breslin, *Surface and Coatings Technology*, 190, 264 (2005).

742 57. M. Tiitu, A. Talo, O. Forsen, O. Ikkala, *Polymer*, 46, 6855 (2005).

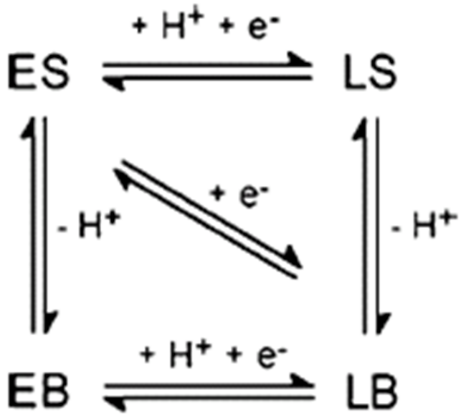
+ H+ + e-
ES
LS
- H+
+ e-
- H+
+ H+ + e-
EB
LB

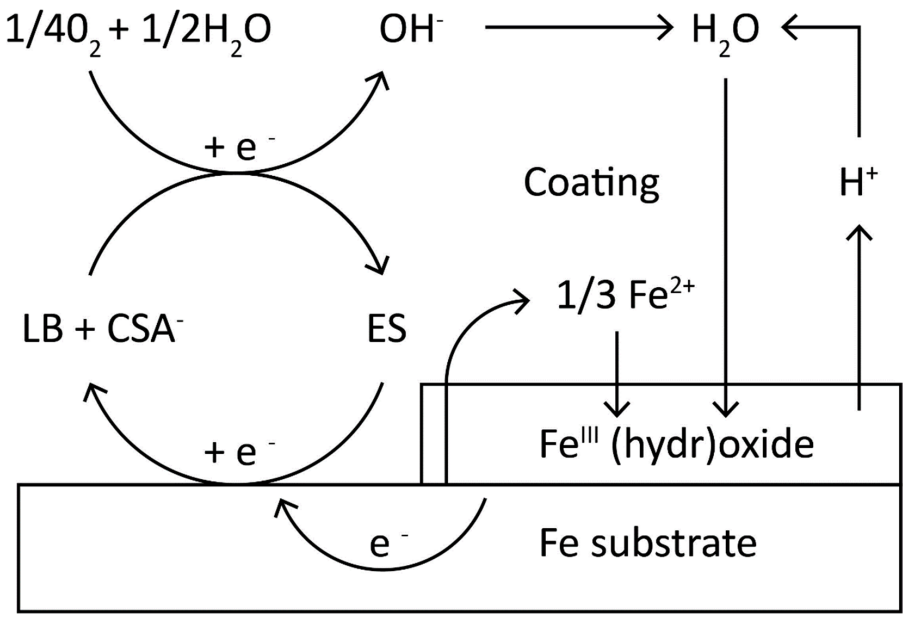
1/40$_2$ + 1/2H$_2$O
OH$^-$
H$_2$O
+ e $^-$
Coating
H$^+$
1/3 Fe^{2+}
LB + CSA$^-$
ES
Fe^{III} (hydr)oxide
+ e $^-$
e $^-$
Fe substrate

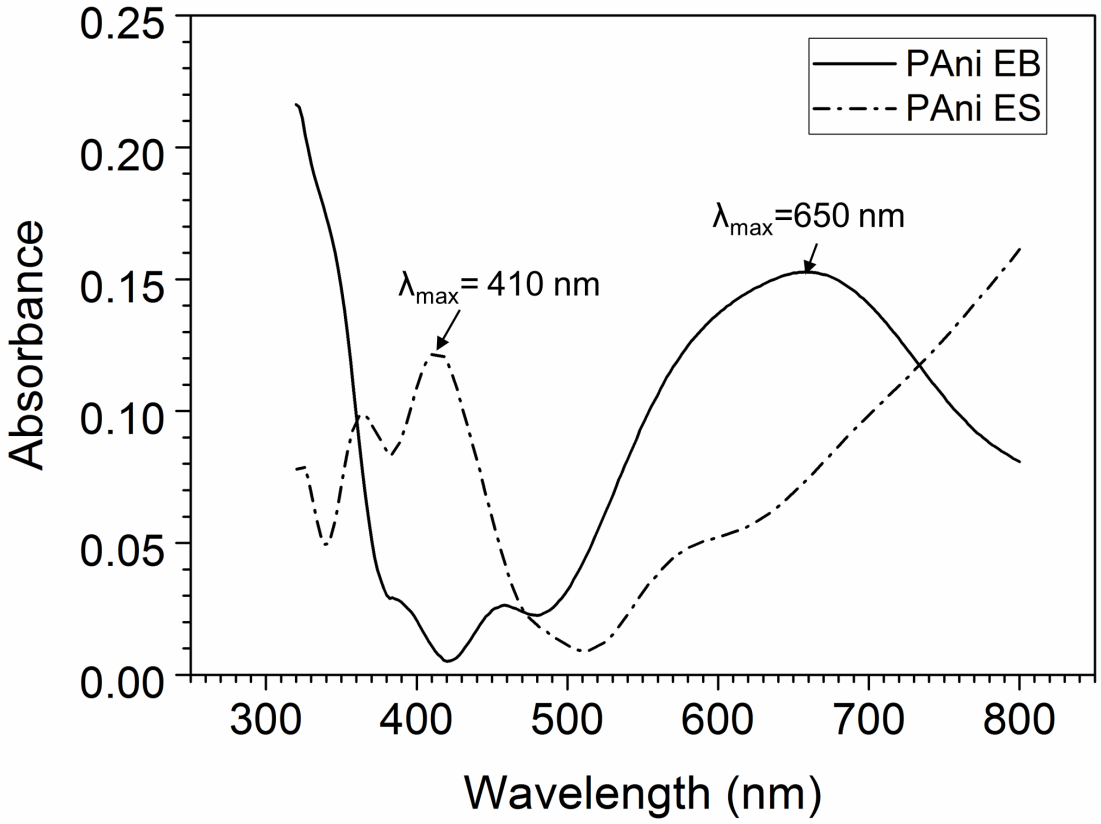
0.25
0.20
0.15
0.10
0.05
0.00
Absorbance
300
400
500
600
700
800
Wavelength (nm)
PAni EB
PAni ES
λmax= 410 nm
λmax=650 nm

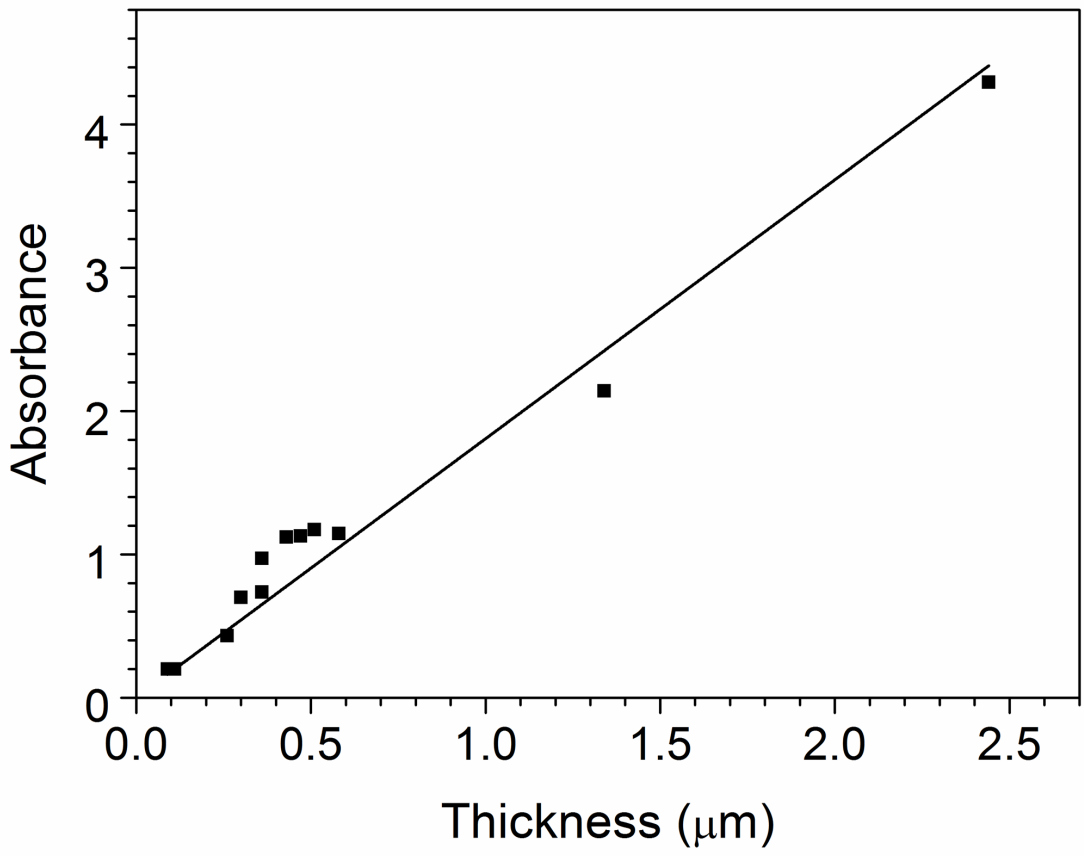
Absorbance
Thickness (μm)
0
1
2
3
4
0.0
0.5
1.0
1.5
2.0
2.5

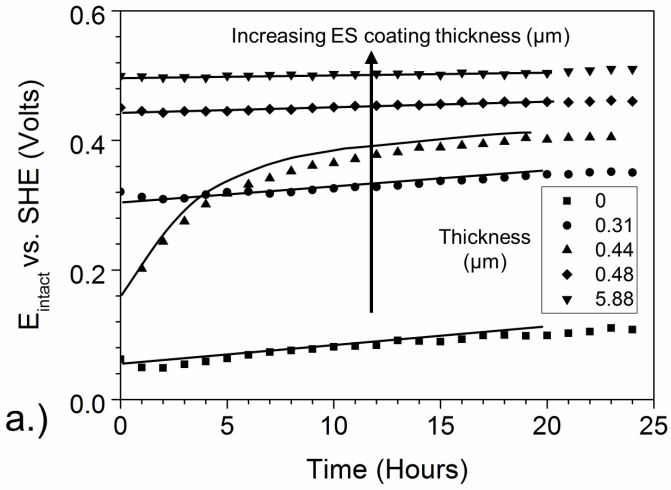
Increasing ES coating thickness (μm)
Thickness (μm)
0
0.31
0.44
0.48
5.88
E_{intact} vs. SHE (Volts)
Time (Hours)
a.)

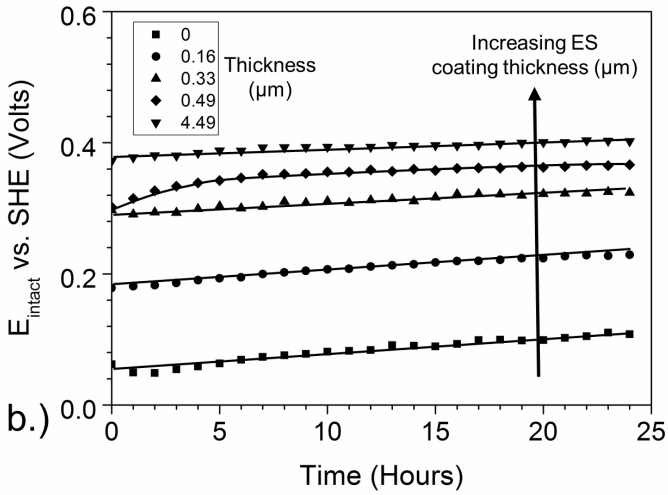
0
0.16
0.33
0.49
4.49
Thickness (μm)
Increasing ES coating thickness (μm)
E_{intact} vs. SHE (Volts)
Time (Hours)
b.)

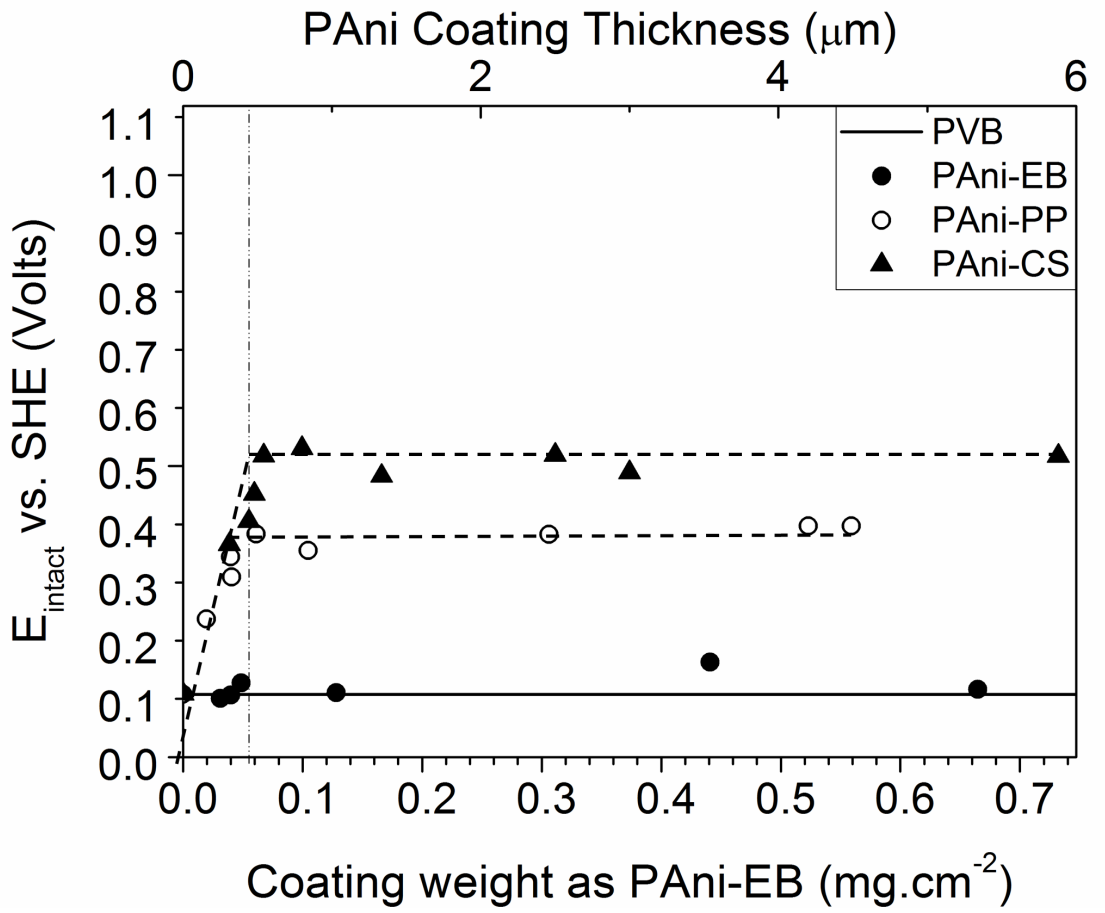
PAni Coating Thickness (μm)
0
2
4
6
PVB
PAni-EB
PAni-PP
PAni-CS
E intact vs. SHE (Volts)
1.1
1.0
0.9
0.8
0.7
0.6
0.5
0.4
0.3
0.2
0.1
0.0
0.0
0.1
0.2
0.3
0.4
0.5
0.6
0.7
Coating weight as PAni-EB (mg.cm-2)

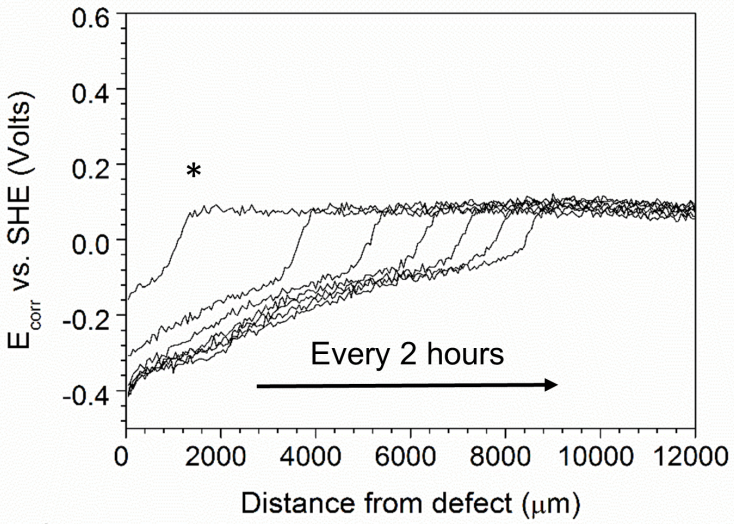
0.6
0.4
0.2
0.0
-0.2
-0.4
E_{corr} vs. SHE (Volts)
*
Every 2 hours
0
2000
4000
6000
8000
10000
12000
Distance from defect (μm)

a.)

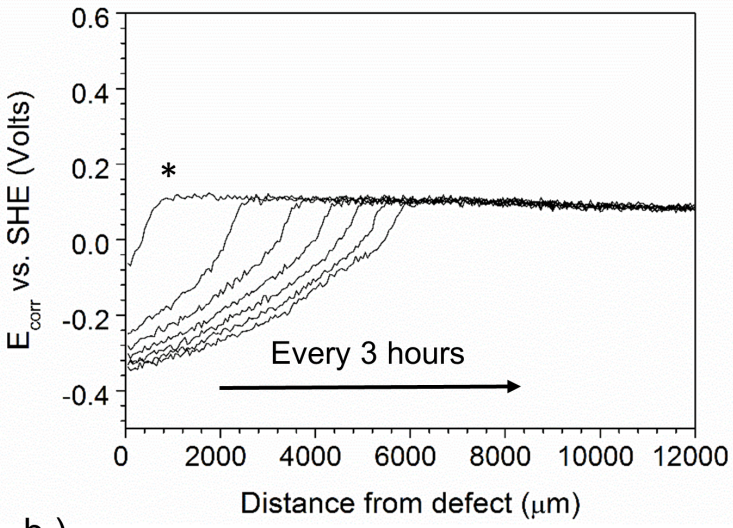
0.6
0.4
0.2
0.0
-0.2
-0.4
E_{corr} vs. SHE (Volts)
*
Every 3 hours
0
2000
4000
6000
8000
10000
12000
Distance from defect (μm)

b.)

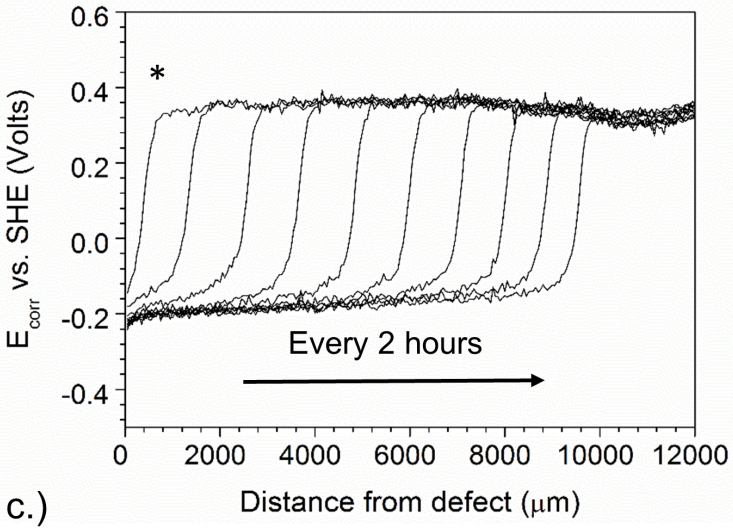
0.6
0.4
0.2
0.0
-0.2
-0.4
E_{corr} vs. SHE (Volts)
*
Every 2 hours
0
2000
4000
6000
8000
10000
12000
Distance from defect (μm)

c.)

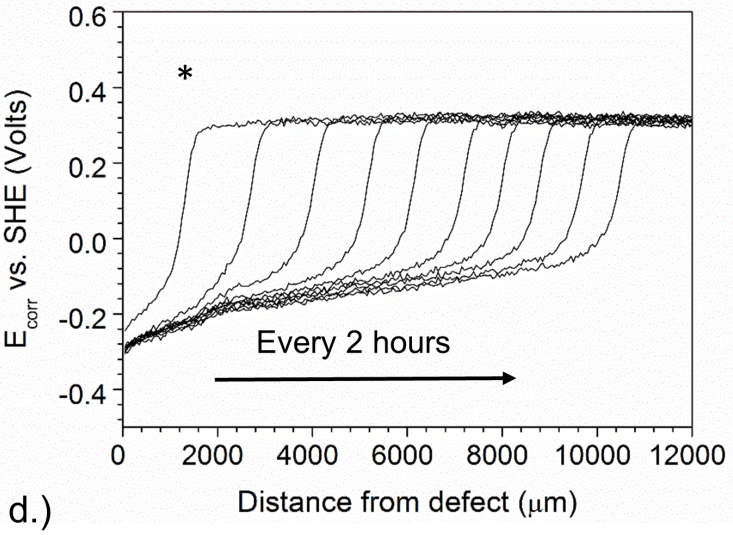
0.6
0.4
0.2
0.0
-0.2
-0.4
E_{corr} vs. SHE (Volts)
*
Every 2 hours
0
2000
4000
6000
8000
10000
12000
Distance from defect (μm)

d.)

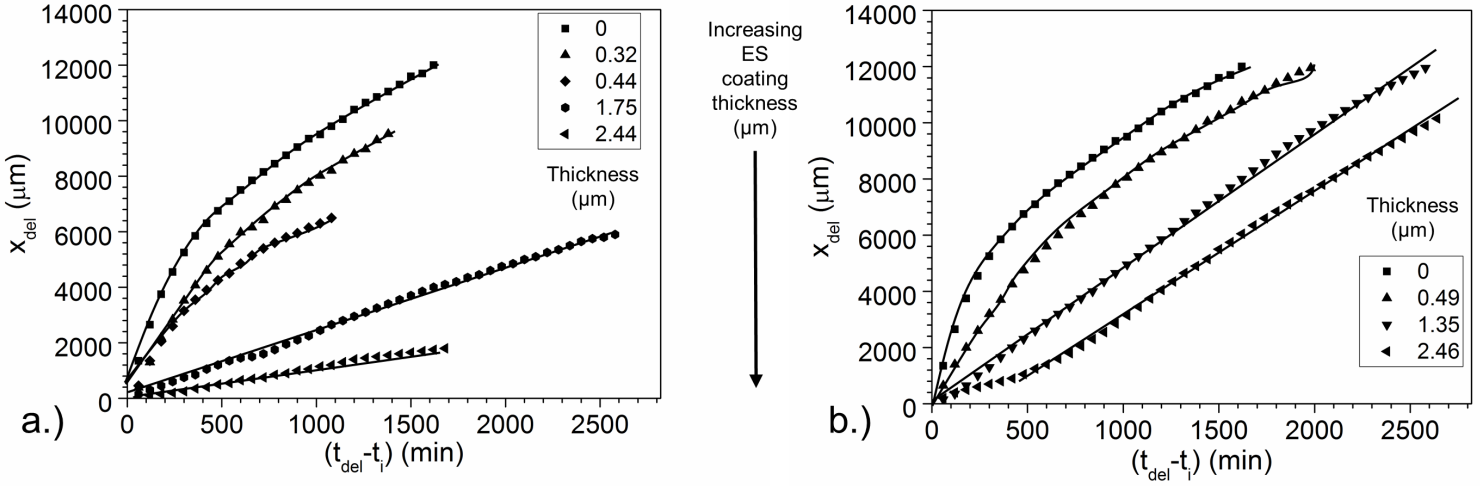
a.)
b.)
x_{del} (µm)
$(t_{del}-t_i)$ (min)
Thickness (µm)
0
0.32
0.44
1.75
2.44
0.49
1.35
2.46
Increasing ES coating thickness (µm)

a.)

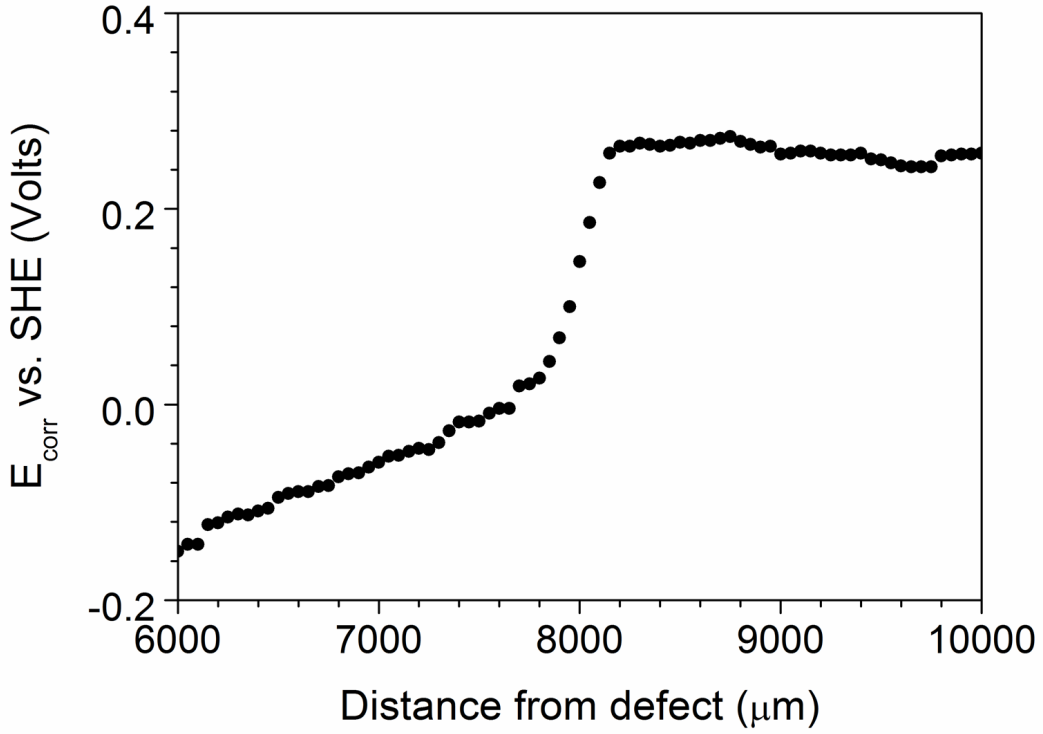
0.4
0.2
0.0
-0.2
E_{corr} vs. SHE (Volts)
6000
7000
8000
9000
10000
Distance from defect (μm)

b.)


PAni-EB
PAni-LB
PAni-ES

c.)

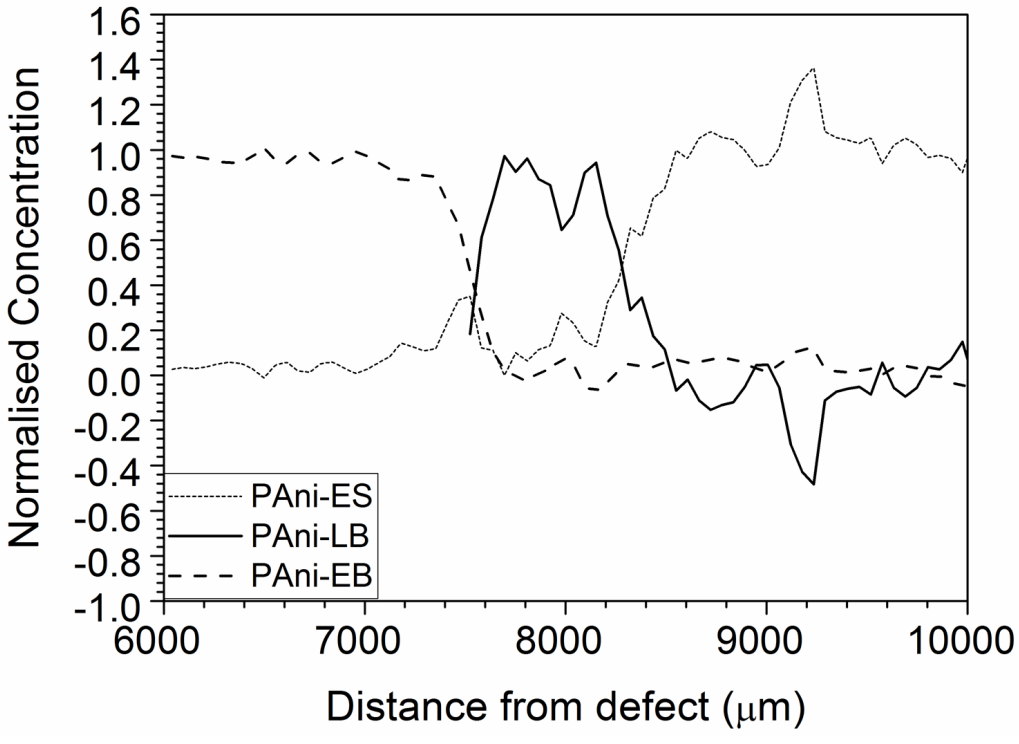
1.6
1.4
1.2
1.0
0.8
0.6
0.4
0.2
0.0
-0.2
-0.4
-0.6
-0.8
-1.0
Normalised Concentration
PAni-ES
PAni-LB
PAni-EB
6000
7000
8000
9000
10000
Distance from defect (μm)

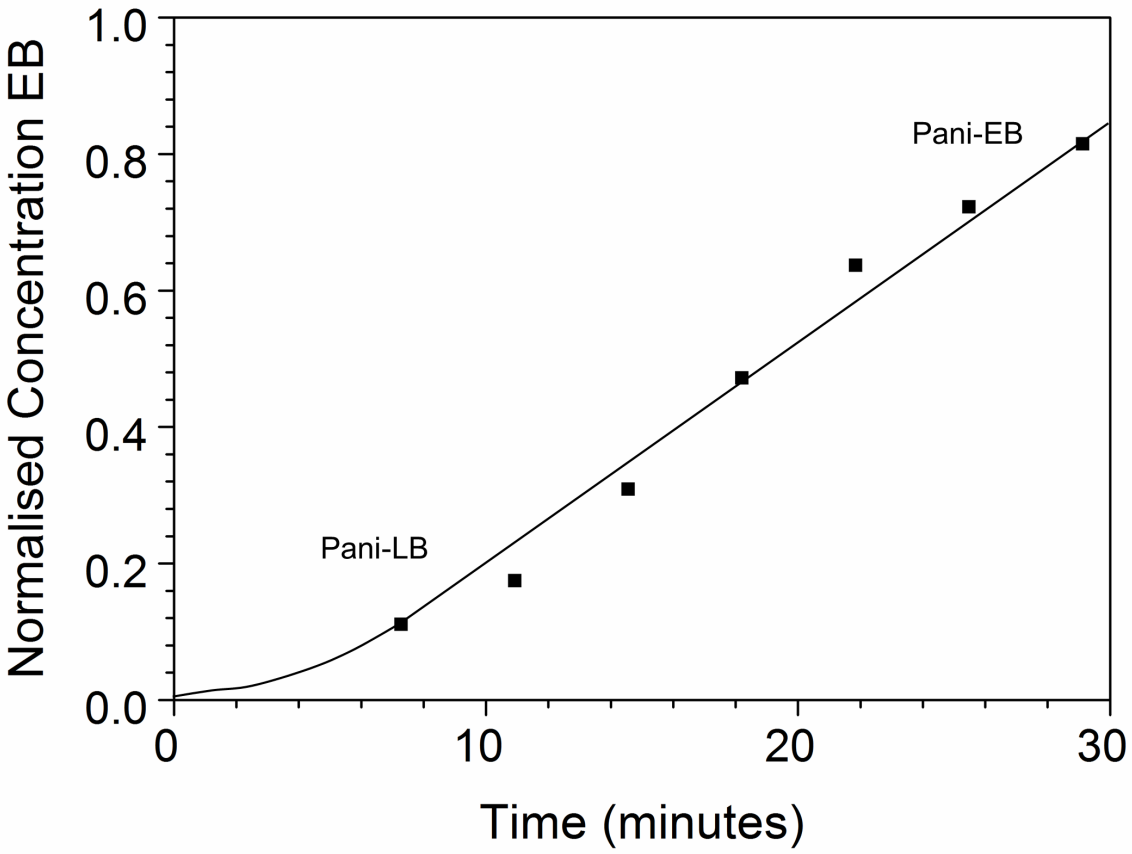
Normalised Concentration EB
1.0
0.8
0.6
0.4
0.2
0.0
0
10
20
30
Time (minutes)
Pani-LB
Pani-EB

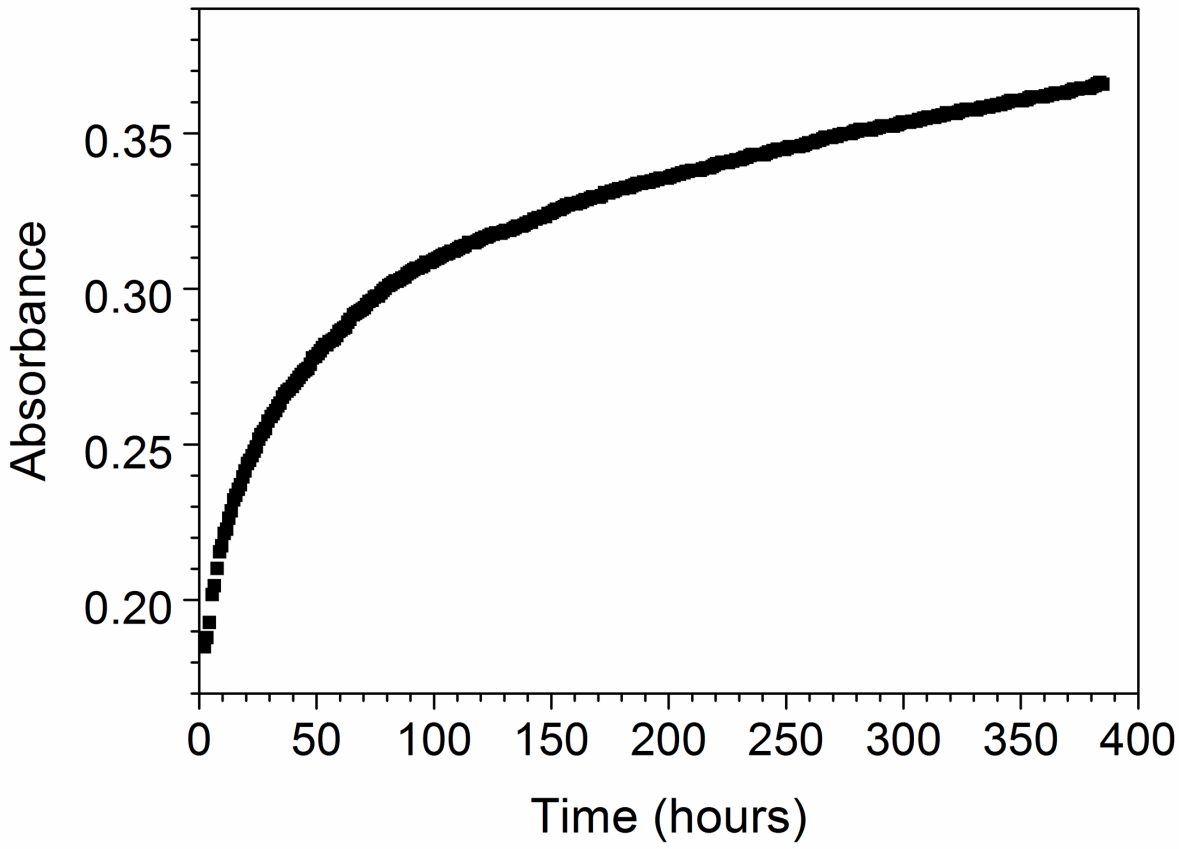
Absorbance
0.35
0.30
0.25
0.20
0
50
100
150
200
250
300
350
400
Time (hours)

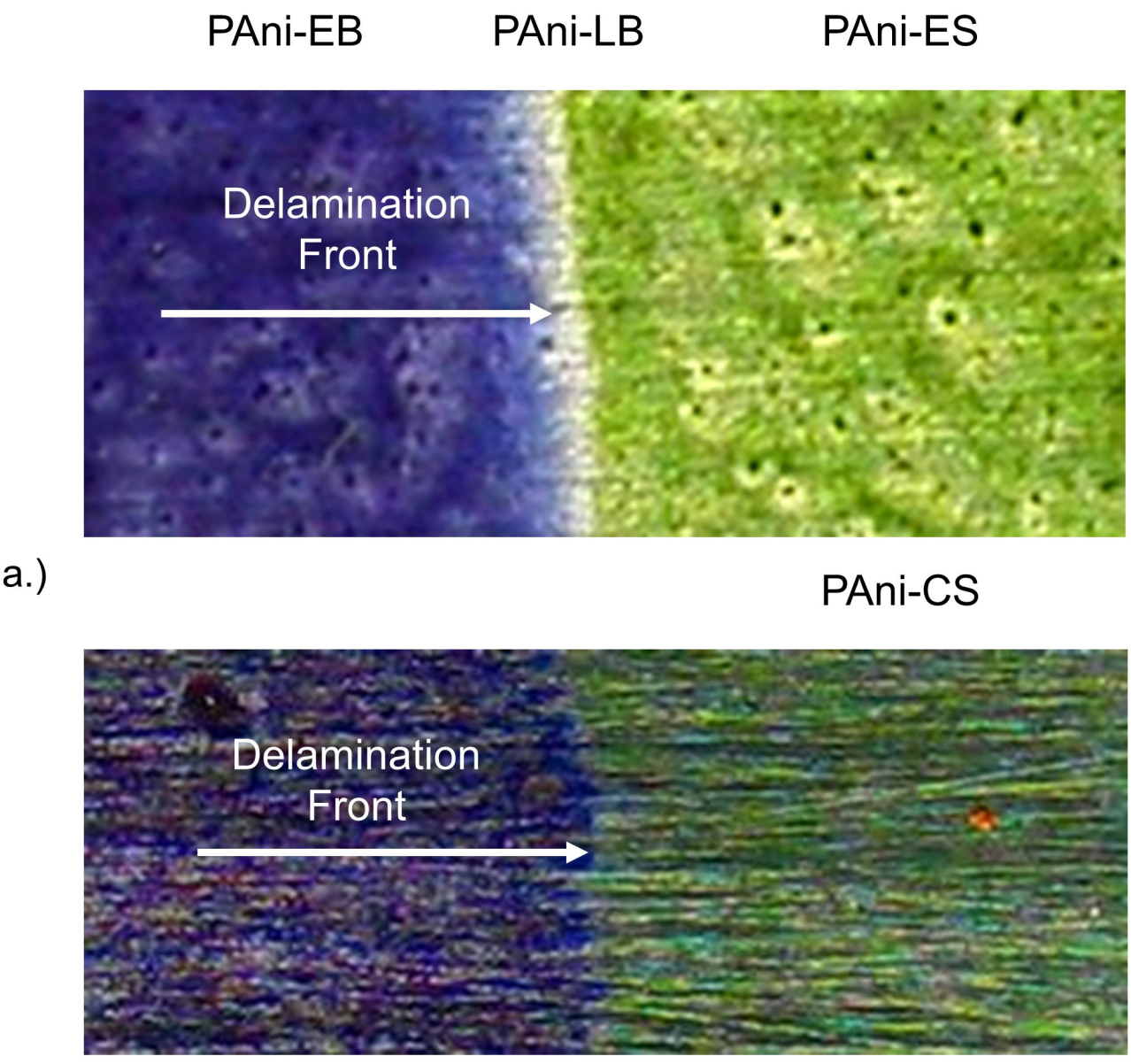
PAni-EB
PAni-LB
PAni-ES
Delamination Front
a.)
PAni-CS
Delamination Front
b.)
PAni-PP
1 mm

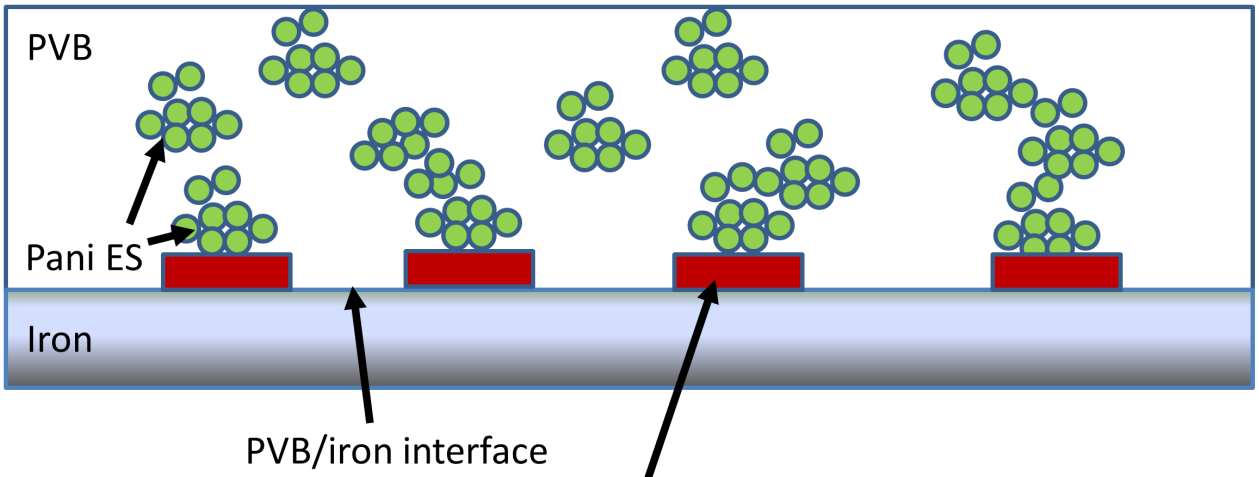
PVB
Pani ES
Iron
PVB/iron interface
PAni ES/iron interphase

a.)

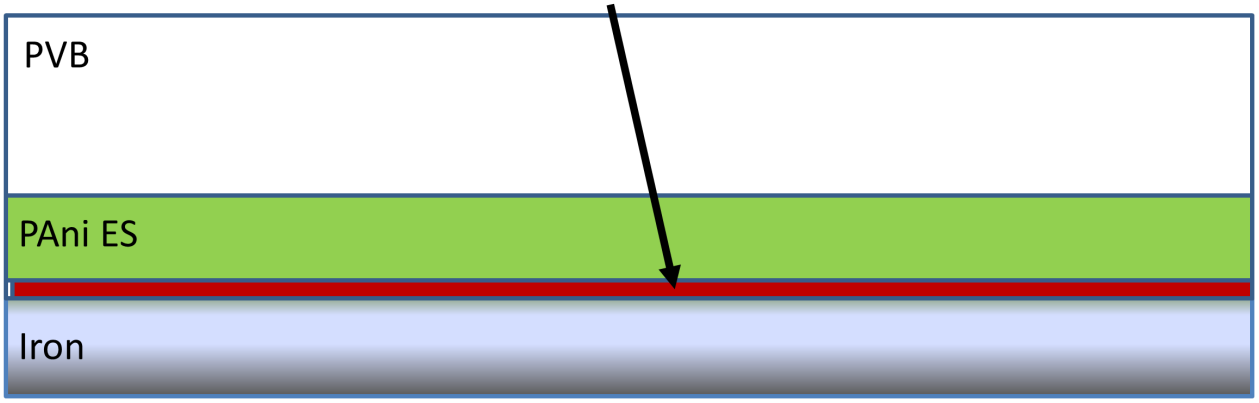
PVB
PAni ES
Iron

b.)

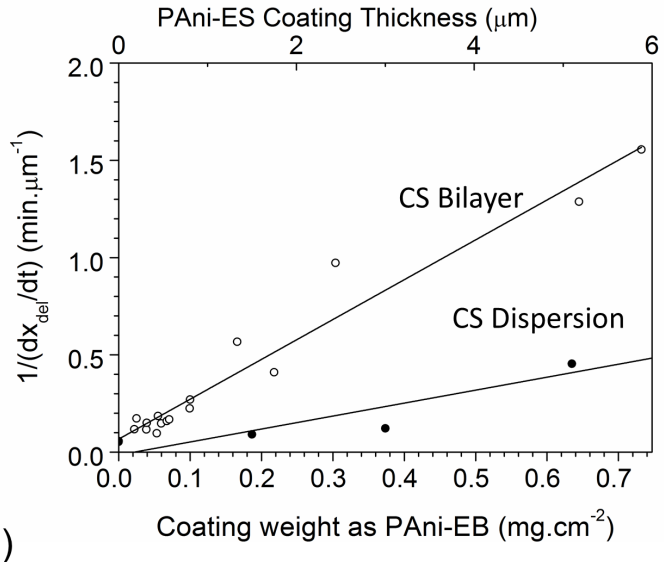
PAni-ES Coating Thickness (μm)
0
2
4
6
2.0
1.5
1.0
0.5
0.0
1/(dx_del/dt) (min.μm^-1)
CS Bilayer
CS Dispersion
0.0
0.1
0.2
0.3
0.4
0.5
0.6
0.7
Coating weight as PAni-EB (mg.cm^-2)

a.)

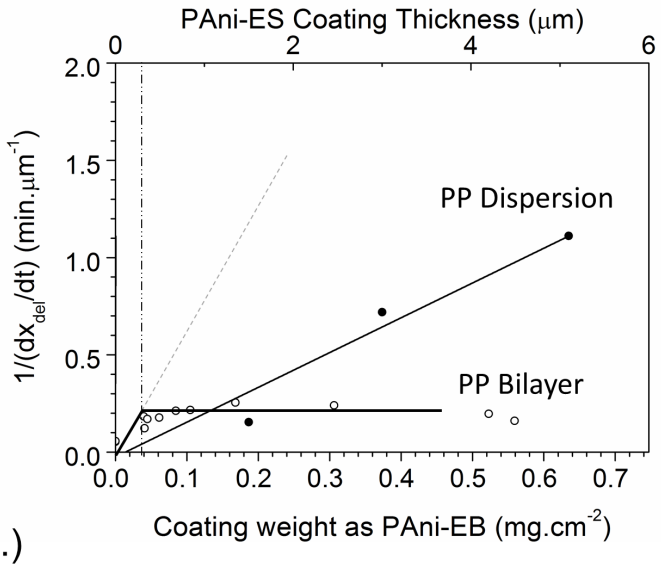
PAni-ES Coating Thickness (μm)
0
2
4
6
2.0
1.5
1.0
0.5
0.0
1/(dx_del/dt) (min.μm^-1)
PP Dispersion
PP Bilayer
0.0
0.1
0.2
0.3
0.4
0.5
0.6
0.7
Coating weight as PAni-EB (mg.cm^-2)

b.)